MICHIGAN STATE UNIVERSITY

CYCLOTRON LABORATORY

DYNAMICS OF RELATIVISTIC HEAVY ION COLLISIONS AND QUARK-GLUON PLASMA FORMATION

J.J. MOLITORIS AND H. STÖCKER

TO BE PUBLISHED IN THE PROCEEDINGS OF THE
5th ADRIATIC INTERNATIONAL CONFERENCE ON
NUCLEAR PHYSICS-HEAVY ION REACTIONS
HELD SEPTEMBER 24-29, 1984
IN HVAR, YUGOSLAVIA.

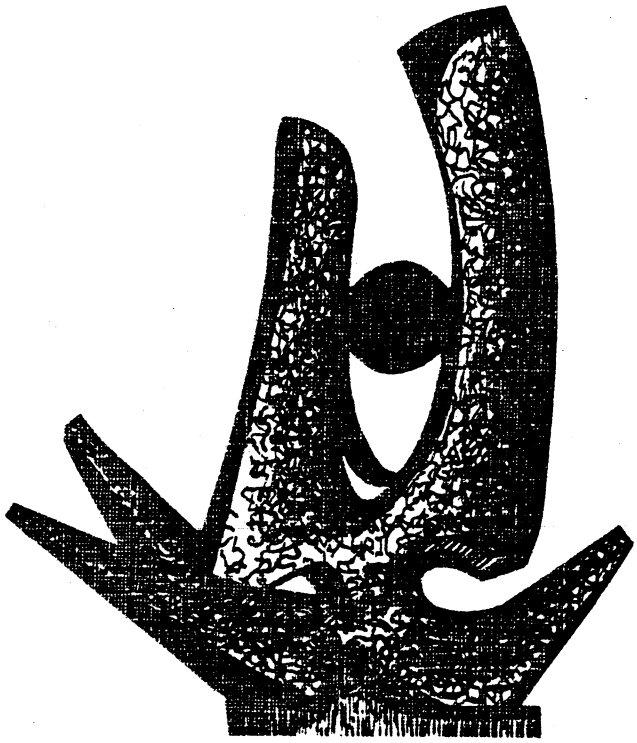

NOVEMBER 1984

MSUCL 495

MSUCL-495
November 1984

Dynamics of Relativistic Heavy Ion Collisions and Quark- Gluon Plasma Formation*

J.J. Molitoris and H. Stöcker

National Superconducting Cyclotron Laboratory and
Department of Physics and Astronomy, Michigan State University
East Lansing, Michigan 48824

ABSTRACT

We review various theoretical approaches which have recently been developed to describe high energy nucleus-nucleus collisions. These models are applied to recent high multiplicity 4π selected data on pion production and collective flow from the Streamer Chamber and the Plastic Ball. The intranuclear cascade model, classical equation of motion simulations, the fluid dynamic model, the Vlasov Uehling-Uhlenbeck theory, and the time dependent Dirac equation with meson field dynamics are discussed. A comparison of the various theoretical approaches to the data on flow, pion formation and entropy production indicates a surprisingly stiff nuclear equation of state. It is pointed out that - if the nuclear stopping observed at BEVALAC energies persists up to energies of 10 GeV/N - a deconfined baryon rich quark gluon plasma might be formed at the facilities presently under construction at Brookhaven and CERN.

* Supported by the U.S. National Science Foundation.

Little is known to date about the properties of nuclear matter at finite temperatures and densities other than the ground state density, $n_0 = 0.15\ fm^{-3}$. Nuclear matter may have a rich structure in the hithero unexplored domain of high excitation energies and compression. For example, there are conjectures about a nuclear liquid- vapor phase transition at $T \sim 20$ MeV and $n < 0.5\ n_0$, about abnormal nuclear matter (density isomers and pion condensates) at high densities, $n \sim 3 - 5\ n_0$, and the possibility of the deconfinement phase transition from hadronic matter into the quark- gluon plasma at $n > 5 - 10\ n_0$ and/or $T \sim 100 - 200$ MeV. Experimental information on this unexplored domain is being sought by analyzing high energy collisions of heavy nuclei: if the nuclei can stop each other, high energy densities can be obtained for $t \sim$ several 10^{-23} seconds. Collisions of massive equal nuclei, however, could not be studied experimentally in the past. Only recently have ions with mass $A > 40$ been accelerated at the BEVALAC to bombarding energies between 100 MeV/N to 2 GeV/N.

The most important question to be answered by theorists is how the information on the early hot and compressed stage of the collision can be extracted from the emission pattern of the reaction products. One of the first predicted signatures for nuclear stopping and compression is the sidewards flow of nuclear matter in head-on collisions of massive equal nuclei[1] (see Fig. 1). In contrast to the density and temperature, which first increase, but then steadily decrease during the course of the collision, the predominant emission pattern is established at the time of highest compression (i.e. at the highest pressure) and stays constant during the expansion. Pion- and entropy production exhibit the same time dependence, hence they can also yield information on the high density stage of the reaction. One may view the flow as a barometer, the pion yield as a calorimeter, and the entropy as a measure for the number of degrees of freedom for high density matter.

In this paper we want to give a survey of recent experimental and theoretical developments in the field of high energy heavy ion reactions. First we give an overview of the various theoretical approaches developed to describe the complicated collision dynamics, discussing also the recent 4π experiments on pion production and flow. Next we discuss the status of recent attempts to determine the entropy

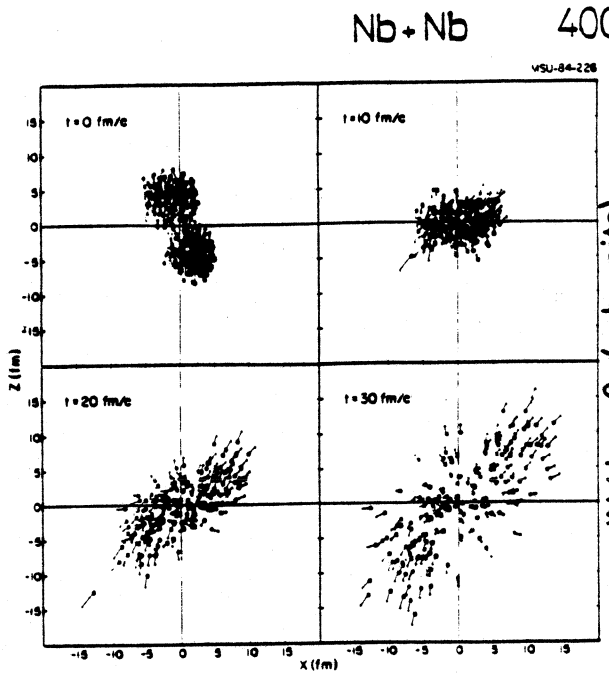

Fig. 1

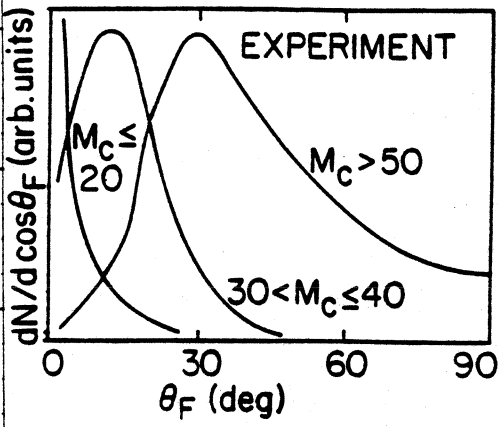

Fig. 2a

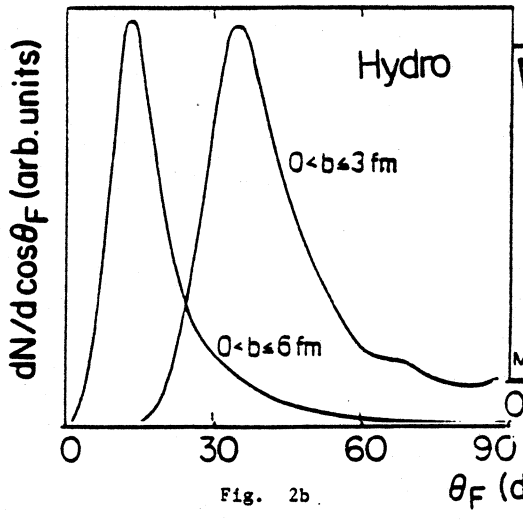

Fig. 2b

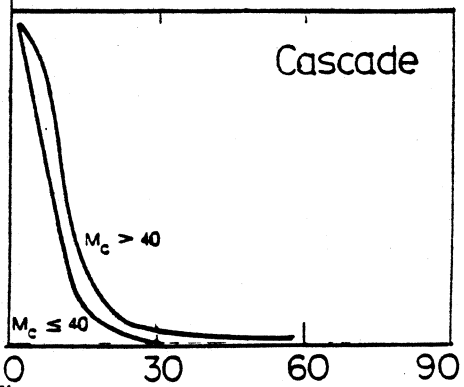

Fig. 2c

from light and medium mass fragment abundancies. Finally, we turn to the high energy domain, $E_{Lab} >> 1$ GeV/N. We discuss the deconfinement phase transition from hadron matter into the quark gluon plasma, with particular emphasis on the available energy densities, the transition parameters and the space time structure of the high energy density regions.

Preferential sidewards emission of fragments from central collisions of high energy nuclei had been reported previously for very asymmetric reactions, e.g. C + Ag and Ne + U: early particle track detector experiments[2] yielded peaks in the angular distribution of alpha particles emitted from central C+Ag reactions, and the double differential cross sections of light fragments (p,d,t) emitted from high multiplicity selected collisions of Ne (393 MeV/n) + U exhibit sidewards maxima,[3] in accord with predictions of the fluid dynamical model.[4]

Recently it has been proposed to observe the collective flow directly via a kinetic energy flow analysis[5,6] on an event-by-event basis. The sensitivity[6] of the flow analysis for very heavy systems to the properties of nuclear matter at high densities and excitation energies is particularly fascinating. The basic idea of the flow analysis is to measure event-by-event the momenta of all (charged) particles. Such an analysis can be done experimentally only with 4π detector systems such as emulsion, streamer chamber, or the plastic ball. Once this information is available, the momenta are transformed into the center-of-momentum frame and the direction of the maximum kinetic energy flow is determined by performing a principal axis transformation.

The kinetic energy flow tensor K_{ij},

$$K_{ij} = \sum_{\nu} \frac{p_i(\nu)\, p_j(\nu)}{2 \quad m(\nu)} \qquad (1)$$

insures that composite fragments ν contribute to the matter flow tensor with the correct weight relative to nucleons.[5-7] For the reaction ^{93}Nb (E_{lab} = 400 MeV/N) + ^{93}Nb we show in fig. 2a the experimental flow angular distribution.[8]

A relativistic quantum field theoretical description of the complicated many body dynamics of high energy nuclear collisions is, for the time being, not in sight. However, tractable approximations have been developed which allow the study of the collision dynamics. By comparison of the predictions of the different theories with experiments, one can try to infer which of the approximations is most physically reasonable.

1. Intra-Nuclear Cascade Simulations

The intranuclear cascade model (INC) is a microscopic simulation of the reaction dynamics at high bombarding energies. Nuclear collisions are treated as a superposition of independent NN collisions. Nucleons move on straight line trajectories until they collide with a probability given by free NN scattering cross sections. Momentum and energy are conserved in the collisions and the evolution of the system is followed until the interactions cease. The flow calculations [8,14] done with the standard INC programs[9] result in forward peaked angular distributions, in contrast to the data,[8] and the calculated pion multiplicities [3,9] drastically overestimate the experimental yields (see below). In fig. 2c, we present the INC results on collective flow. Note that the INC yields zero flow angles even at the highest multiplicities, contrary to the experimental data.

These large discrepancies are surprising in view of the success of the cascade model in describing inclusive data[9]. It has been conjectured[3] that the difference between measured pion yields and cascade predictions is due to the neglect of compression energy in the cascade approach.

2. Classical Equation of Motion Approach

We have recently[10] developed a many body equations of motion (EOM) approach to study heavy ion collisions analogous to that of Bodmer et al.,[11] and Wilets et al.[12] Hamilton's equations of motion are solved for an ensemble of A_P+A_T nucleons with simultaneous mutual two-body interactions between all particles:

$$\dot{\vec{p}}_i = - \vec{\nabla}_{r_i} H, \quad \dot{\vec{r}}_i = \vec{\nabla}_{p_i} H . \qquad (2)$$

The Hamiltonian is $H = \sum_{i=1}^{A} \frac{p_i^2}{2m} + \sum_{i<j} V(r)$ where $r=|\vec{r}_i-\vec{r}_j|$ is the distance between nucleons i and j.

The nucleon-nucleon potential consists of two terms, an attractive long range Yukawa interaction, and a repulsive short range core[11,12].

$$V = (V_R\, e^{-K_R \cdot r} - V_A\, e^{-K_A \cdot r})/r. \qquad (3)$$

We have developed such an approach to study collective flow effects and chosen V_R=2970 MeV-fm, V_A = 765 MeV-fm, K_R = 2.66 fm^{-1} and K_A = 1.75 fm^{-1} in a compromise betwen reproducing the np differential scattering cross section and at the same time giving reasonable nuclear radii and binding energies.[10]

In the EOM approach, nuclei are described as an ensemble of protons and neutrons initially distributed randomly throughout a sphere with the nuclear radius $R=1.2\ A^{1/3}$ fm. A metastable ground state has been obtained by allowing the nucleons to drift toward the configuration of minimum energy of the chosen nucleon-nucleon potential.[11] The nucleons are given random Fermi momenta consistent with experimental values which results in an average binding energy of 7 MeV/N.

To simulate a collision process, the nuclei are Galilei-boosted with the respective center of mass momenta at given impact parameter. The equations of motion are integrated numerically. The evolution of a collision at b = 3 fm impact parameter is shown in Fig 1. The resulting sidewards flow can clearly be seen. The individual collisions are analyzed by diagonalizing the kinetic energy flow tensor. The distribution of flow angles $dN/d\cos\theta_F$ is presented in Fig. 2d for two impact parameter intervals. The qualitative and quantitative behavior of the flow pattern in the EOM model is very similar to the behaviour observed previously in hydrodynamics:[13] the flow angle θ_F rises smoothly from 0° at large impact parameters to 90° at b=0. A finite range of impact parameters is sampled to compute the angular distributions of the flow angles, $dN/d\cos\theta_F$. The distribution of flow angles is computed by taking into account the formation of fragments via a 6-dimensinal coalescence model recently developed.[14] We

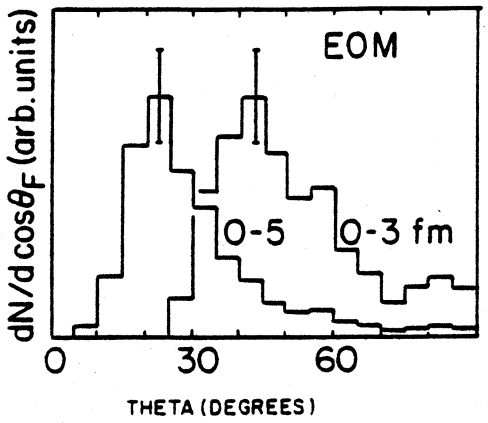

Fig. 2d

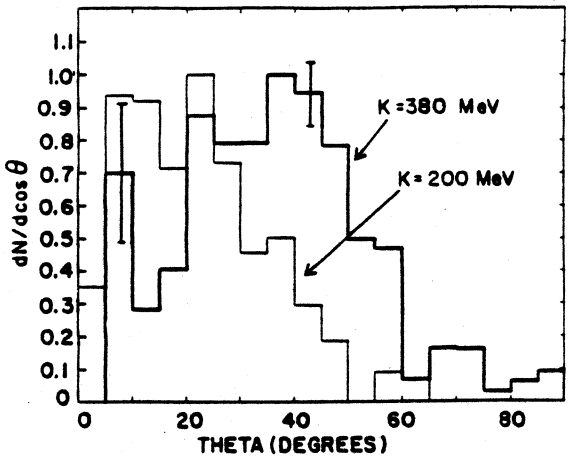

Fig. 3a

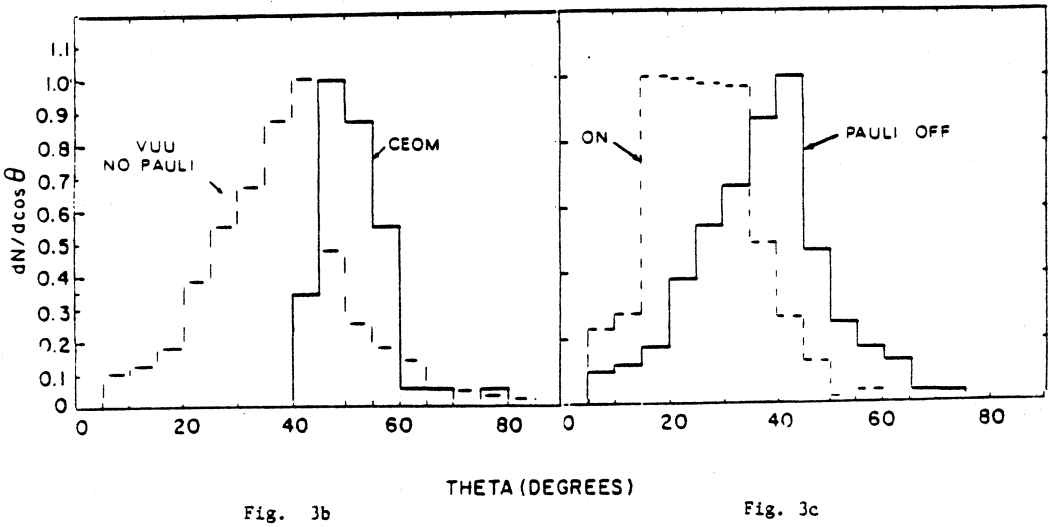

Fig. 3b

Fig. 3c

find roughly the same flow distribution by doing the flow analysis with and without clustering.

This model predicts peaks in the angular distribution of the flow angles which shift to larger angles with increasing multiplicity in agreement with the data. The physical difference between the INC model and the EOM approach, which leads to such distinct predictions, can be traced back to the different treatments of the NN collision process. The INC applies a stochastic 4π scattering at the point of closest approach of straight line trajectories; this allows for substantial transparency. In contrast, the repulsive short range component in the NN potential is a hard core and thus results in an excluded volume effect; thus the nuclei are not as transparent and easily compressible as in the INC. This causes incident nucleons to be deflected away from zones of high density, i.e. small interparticle separations, towards sidewards angles. It is important to point out the role of the binding potential: the potential field keeps the nuclei from expanding before collisions can occur. If binding is neglected as in Cugnon's original program,[9] finite flow angles occur due to sidewards expansion of the unbound projectile and target nucleons because of Fermi motion.[14]

Nuclear Fluid Dynamics

In the hydrodynamic calculations,[4,6,7,13] the reaction volume is divided into cells characterized by a mean flow velocity, $v(r)$, a local temperature $T(r)$, and a local baryon number $n(r)$. The equations of motion are obtained by demanding baryon number, momentum, and energy conservation. When the baryon density in a cell falls below a freezeout value during the expansion it contributes an amount $1/2(\bar{p}_i\bar{p}_j/m + \delta_{ij}T)$ to the flow tensor. Thus, for hydrodynamics F_{ij} is the sum of a collective flow tensor $\bar{F}_{ij}=\bar{p}_i\bar{p}_j/2m$ and a stochastic part $\delta_{ij}E_T/3$.[6]

The general behavior of the flow pattern in the fluid dynamical model is as discussed above for the CEOM approach. The major cause of concern for a direct comparison of the data to the hydrodynamical predictions is, however, the finite multiplicity, $M < 50$, of emitted fragments: there are substantial finite number distortions[15] to the kinetic energy flow analysis for multiplicities $M < 100$. The finite

multiplicity effects have been incorporated into the theory via a Monte Carlo procedure. The detector efficiencies can be folded into the theoretical analysis, thus allowing for an unbiased, direct comparison of theory and data.

Fig. 2b shows the distribution of flow angles, $dN/d\cos\theta_F$. The theoretically obtained[13] high multiplicity triggered events, corresponding to the small impact parameters (b=0 to 3 fm) compare favorably with the high multiplicity selected experimental data. The intermediate multiplicities ($30 < M < 40$) correspond to larger impact parameters, $3 < b < 6$ fm in the hydrodynamical calculation. The experimentally observed decrease of the average flow angle (by $\theta_F = 15°$) is well reproduced by the fluid dynamical calculation.

4. The Vlasov Equation with Uehling Uhlenbeck's Collision Term

This theory explains for the first time simultaneously both the observed collective flow and the pion multiplicity and gives their dependence on the nuclear equation of state in a microscopic approach.[14] Vlasov's equation for the evolution of the single particle distribution function f of a collisionless plasma in a self- consistent mean potential field is supplemented by Uehling- Uhlenbeck's quantum mechanical extension of Boltzmann's two body collision term which respects the Pauli principle (acronym VUU). This extended Boltzmann equation can be written[14,16,17]

$$\frac{\partial}{\partial t} f + \vec{v} \cdot \frac{\partial}{\partial \vec{r}} f - \frac{1}{m} \frac{\partial}{\partial \vec{r}} U(n) \cdot \frac{\partial}{\partial \vec{v}} f = -\int \frac{d^3p_2 d^3p_1' d^3p_2'}{(2\pi)^6} \sigma v_{12} \times$$
$$\times \left[f f_2 (1-f_1')(1-f_2') - f_1' f_2' (1-f)(1-f_2) \right] \delta^3(p+p_2-p_1'-p_2'). \qquad (4)$$

The Vlasov equation is solved by simultaneous numerical integration of the classical equations of motion of 15 parallel ensembles of $A_P + A_T$ test particles, which are initially assigned Fermi momenta and random positions in a sphere of nuclear radius. Two test particles from a given ensemble may undergo s-wave scattering if they approach each other within a distance $d^2 = \sigma/\pi$ and the resulting final states are not Pauli blocked where σ denotes the experimental scattering cross section of protons, neutrons, and pions. The

experimental inelastic scattering cross sections σ are used to calculate pion production and absorption through the delta resonance.

Three different Skyrme parametrizations have been chosen to represent the mean field U:

$$\text{stiff} \quad (K=375 \text{ MeV}) \quad U(n) = -124\, n/n_0 + 70.5(n/n_0)^2 \quad \text{MeV} \quad (5a)$$

$$\text{medium} \quad (K=200 \text{ MeV}) \quad U(n) = -356\, n/n_0 + 303(n/n_0)^{7/6} \quad \text{MeV} \quad (5b)$$

$$\text{supersoft equals (5a) at } n < n_0, \text{ constant for } n > n_0. \quad (5c)$$

The last allows the study of bound nuclei with zero compression energy. U is directly related to the nuclear equation of state via $U(n) = \frac{\partial(nE)}{\partial n}$

This method has been tested in various ways. First, inclusive spectra of protons emitted from high energy heavy ion reactions have been calculated. They are compared to recent data[17,18] in Fig. 4. Second, proton induced pion production on nuclear targets has been studied. The absolute yields, the target mass dependence and the large (factors of 5) difference between the π^+ and π^- yields as well as the pion spectra are well reproduced.[14]

The pion multiplicities from central collisions of Ar (0.4 - 1.8 GeV/N) + KCl are shown in Fig. 9 as a function of the bombarding energy.[3,9] The VUU theory with the stiff equation of state (5a) plus phase space Pauli blocker compares well with the data[19], while the 'cascade mode' (5c) overestimates the pion yields by factors > 2 at energies up to 1 GeV/N, just like the INC calculations[9,19]. The drop in the pion yield is found to be due to the transformation of kinetic energy into potential energy during the high density phase of the reaction as well as due to Pauli blocking. To check the sensitivity of the pion yields to the equation of state, the calculations have been repeated with the medium potential (5b). At 772 MeV/N one finds $\langle \pi^- \rangle$ = 2.45±0.09 and 2.13±0.07 with the medium and the stiff equation of state, respectively[14], as expected intuitively.

We have also have investigated the sensitivity of the pion yields in the hydrodynamic model, using a Hagedorn (pions plus resonance gas) equation of state with a quadratically increasing nuclear compression energy, $E_c(n) = (K/18)\,(n/n_0 - 1)^2$. The results are shown in Fig. 10: We

find a similar 10- 20% dependence as with the VUU method. Also we observe that only a rather stiff equation of state with K = 330 MeV can reproduce the data at the higher energies, in agreement with our conclusion from VUU.

The sidewards peaking (Fig. 2a) observed in multiplicity selected Nb(400 MeV/N)+Nb collisions[8] has also been studied. Fig. 3a shows the flow angle distribution[14] for Nb(400MeV/N)+Nb for b=1 fm impact parameter with the medium and the stiff equation of state; we find a strong effect of the equation of state on the flow angle distribution. From the medium equation of state we do not obtain flow angles as large as experimentally observed. This might well be interpreted as additional experimental evidence for a surprisingly stiff nuclear equation of state, just as the pion yields above and the entropy values discussed below. However, to draw a quantitative conclusion we would need to compare the data to the theoretical results after they have been put through the Plastic Ball efficiency filter. Fig. 3c shows the large effect due to turning on/off the Pauli principle. It is interesting that the Pauli principle makes such a large difference even at these high energies. By neglecting the Pauli principle we make contact with the CEOM method; the difference in the theories is mainly due to the 4π random scattering style. We expect the VUU peak to narrow if a repulsive 2π scattering style is introduced. In fig. 3b, we compare the VUU theory with Pauli off and the CEOM method at b=2 fm.

One can also turn on/off the collision term to see the effect of two body collisions. With the collision term off, we recover the Vlasov equation. In fig. 5, we show the dramatic effect of the collision term on the momentum space distributions for Ar (137 MeV/N) +Ca. Fig. 5a shows the initial configuration, while fig. 5b and 5c show respectively the final results without and with collision term.[18]

A flow analysis may also be undertaken for asymmetric collisions. Recent experimental data[20] for Ar (772 MeV/N) +Pb are shown in fig. 6a. Here the experimenters have used the momentum flow tensor:

$$F_{ij}=(\Sigma_\nu p_i(\nu)p_j(\nu)/|p(\nu)|)/\Sigma_\nu|p(\nu)| \qquad (6)$$

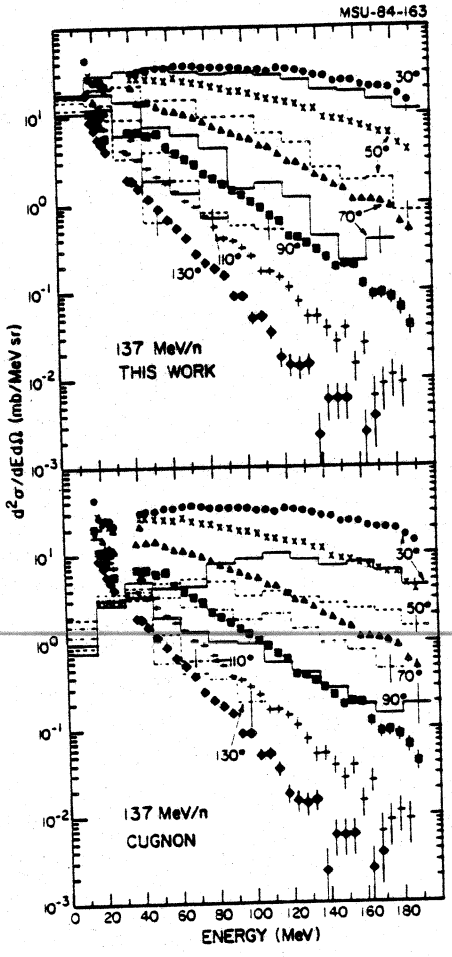
MSU-84-163
137 MeV/n
THIS WORK
137 MeV/n
CUGNON
30°
50°
70°
90°
110°
130°
$d^2\sigma/dEd\Omega$ (mb/MeV sr)
ENERGY (MeV)

Fig. 4

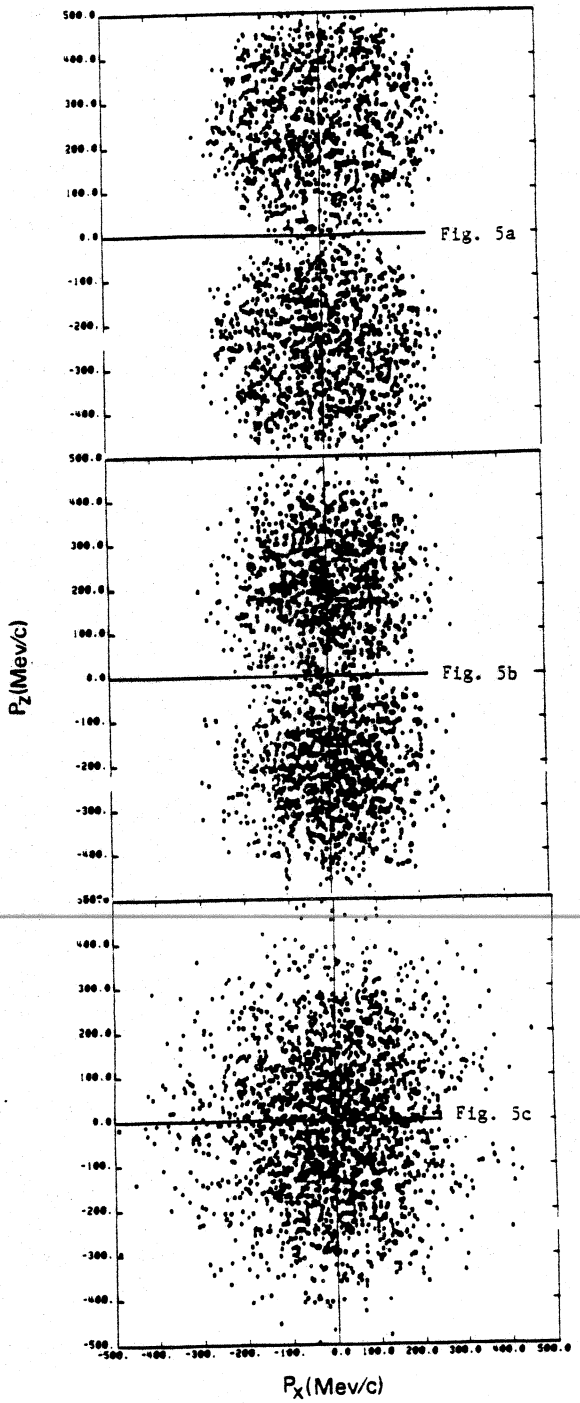
Fig. 5a
Fig. 5b
Fig. 5c
P_z(Mev/c)
P_x(Mev/c)

In fig. 6b and 6c, the INC[23] and fluid dynamical[13] models are compared with the experimental data. Fig. 6d demonstrates that this difference between high and low multiplicity events is also explained by the Vlasov-Uehling-Uhlenbeck[14,21] theory; however this figure is not directly comparable to experimental data since we have done the momentum flow analysis on all protons in the NN center of mass frame. For asymmetric collisions, we advocate that a flow analysis is done in this frame, but only for $p_z > 0$.

5) Time-Dependent Dirac Equation With Meson Mean Field Dynamics

This model consists of nucleons obeying the time-dependent Dirac equation, of a classical spin zero attractive meson field (sigma) obeying the Klein Gordon equation, of a spin one repulsive meson field (omega) obeying the Proca equation and a meson-baryon interaction between them.[22,23] The resulting coupled field equations are solved simultaneously in a mean field approximation. Similar models have been studied for the static case by Walecka.[22] The theory is treated in the Hartree approximation which yields an effective Lagrangian. The masses and coupling constants for the mesons are phenomenological and are adjusted to fit static nuclear matter properies.[22]

The model Lagrangian density is

$$\mathcal{L} = \int d^3r \{ \hbar c \bar{\psi} (i\gamma^\nu \partial_\nu - \frac{m_B c}{\hbar}) \psi - \frac{1}{2} (\hbar c)^2 [\partial_\nu \Phi \partial^\nu \Phi - (\frac{m_S c}{\hbar})^2 \Phi^2] - \frac{1}{2} (\hbar c)^2 [\frac{1}{2} F_{\mu\nu} F^{\mu\nu} - (\frac{m_V c}{\hbar}) V_\mu V^\mu] - \hbar c \, g_s \Phi \bar{\psi} \psi - \hbar c \, g_\nu V^\nu \bar{\psi} \gamma_\nu \psi \quad (7)$$

where $F_{\mu\nu} = \partial_\nu V_\mu - \partial_\mu V_\nu$, Φ=σ-field, V=ω-field, and ψ=baryon field.

The classical equations derived from the Lagrangian density propagate the mesonic mean fields. Thus the baryonic field equation can be treated exactly by single nucleon propagation, and Slater determinants will remain so at all times.

Heavy ion collisions have recently been calculated with this approach.[23] Figure 7 shows the baryon density in momentum space for O + O at 600 MeV/N and b=2 fm. The momentum space rotation (scattering) takes place mainly between 6.2 and 9.1 fm/c. The expansion phase follows. The filling of the phase space in the center of mass is more complete at 300 MeV/N and smaller at 1200 MeV/N.[23]

This partial filling of the zero momentum states can be contrasted with hydrodynamic calculations[13] and Boltzmann equation results[14,17] where complete filling is observed. Experiments for Ca+Ca, Nb + Nb,[8] and Ar + Pb [20] suggest that more particles do indeed fill the zero momentum region than predicted by this calculation. The partial filling seen here could be due to the short interaction time in this light system. The inclusion of two-body scattering terms in addition to the mean fields could also increase the filling.

We show in Fig. 8 a quantity[8,23] which is less sensitive to the filling and which illustrates the sidewards flow. The reaction plane mean transverse momentum[8] shows peaks near the fragments initial momenta and correspond to mean flow angles of 9° and 16° for b=1 and 2. These are modest values when compared to experiments for heavier nuclei.[8] Again the low mass of the fragments could be responsible for this. Calculations for Ca+ Ca would be desirable and are presently difficult to do because of the computing time.

6. Entropy Production

All the diverse theoretical frameworks dicussed have one prediction in common: the high density stage is followed by a rapid expansion of the system. The compressed matter expands due to its high internal excitation and the temperature drops substantially. Hydrodynamic as well as cascade calculations have shown, however, that the entropy of the system stays approximately constant during the expansion. Hence it is of great interest to find an experimental observable related to the entropy, since this can yield insight into the properties of the system at high densities and temperatures. It was pointed out that entropy can be related to cluster production, in particular to the ratio of deuteron yield to proton yield R_{dp}.

It has been pointed out[6,8,18] that composite fragments must be incorporated into the entropy vs. fragment yield calculation, in particular particle unstable excited nuclei, $A^* \rightarrow (A-1)+p$, which distort the equilibrium yields of protons substantially. Furthermore, the inclusion of intermediate mass fragments, $A \geq 3$, has been shown to alter the extracted entropy values. On the experimental side, it has been shown recently that the use of inclusive yields of light fragments can be very misleading for an extraction of the entropy: it is found that

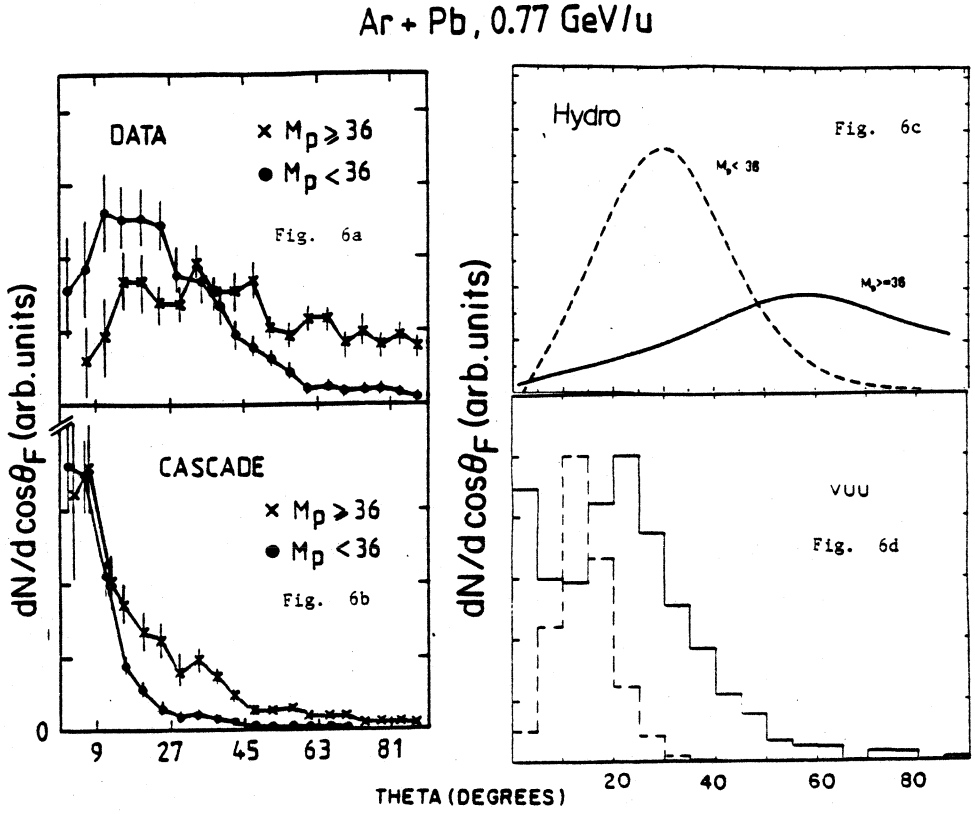
Ar + Pb, 0.77 GeV/u
DATA
× Mp ≥ 36
● Mp < 36
Fig. 6a
CASCADE
× Mp ≥ 36
● Mp < 36
Fig. 6b
dN/d cosθF (arb.units)
0
9
27
45
63
81
Hydro
Fig. 6c
Mp< 36
Mp>=36
VUU
Fig. 6d
20
40
60
80
THETA (DEGREES)

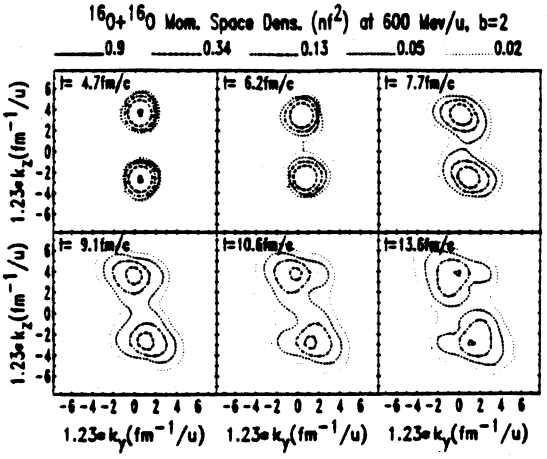
16O+16O Mom. Space Dens. (nf2) at 600 Mev/u, b=2
0.9
0.34
0.13
0.05
0.02
t= 4.7fm/c
t= 6.2fm/c
t= 7.7fm/c
t= 9.1fm/c
t=10.6fm/c
t=13.6fm/c
1.23∗kz(fm−1/u)
1.23∗ky(fm−1/u)

Fig. 7

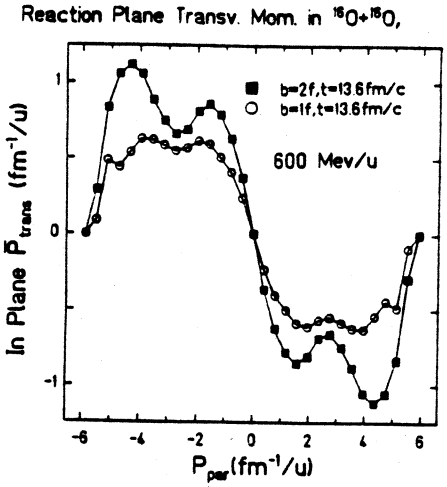
Reaction Plane Transv. Mom. in 16O+16O,
b=2f,t=13.6fm/c
b=1f,t=13.6fm/c
600 Mev/u
In Plane Ptrans (fm−1/u)
Ppar(fm−1/u)

Fig. 8

the proton to deuteron ratios depend strongly on the multiplicity in an event.[8]

A quantum statistical model which takes into account simultaneously particle unstable nuclides and ground state nuclei up to mass 25, as well as Bose condensation of the integer spin nuclides, excluded volume effects, pions and the delta resonance has been developed.[6]

In contrast to expectations from the data, the calculated R_{dp} values are not much smaller than unity, but in fact approach one at $S/A \approx 2$. However, due to the subsequent sequential decay of the particle unstable nuclides, R_{dp} drops substantially after the fragments have been emitted from the system. The rise of "S" or depletion of R_{dp} predicted to occur at intermediate energies E_{LAB}<100 MeV/n, has indeed been observed recently and lends support to our calculation. The triton (and ^{3}He)-to-proton ratios R_{tp} and $R_{^3Hep}$ show a very similar dependence on the entropy S/A as R_{dp}. They exhibit a maximum $R^{max}_{^3Hep}=R^{max}_{tp}\approx 0.3$ around $S/A \approx 2$-3, and are also nearly independent of the breakup density ρ_{bu}. The calculated R_{tp} values agree well with the data.

The increase in deuteron production with increasing multiplicity can be described by the coalescence model taking into account both the size of the deuteron and the volume of the participant region.[8]

The analysis of the Nb(400 MeV/N)+Nb data shows approximately the same cluster production as in 400 MeV/N Ca+Ca at the same multiplicity number of participants. Furthermore, a comparison of the cluster production at different bombarding energies but fixed number of participants yields a decrease of R_{dp} with increasing energy.[8] Hence, the asymptotic (extracted to infinite multiplicity) "d" to "p" values may be used to extract the entropy. Fig. 11 shows the entropy as a function of the bombarding energy calculated in the hydrodynamic model for a stiff Walecka and a soft Boguta equation of state. The entropy values as extracted from the asymptotic value of d/p observed for Nb+Nb at 400, 650 MeV and Ca+Ca at 1050 MeV/u are shown for comparison.[8] The data seem to indicate a rather stiff nuclear equation of state in qualitative agreement with the results from pion production and collective flow.

7. Deconfinement in the Baryon Rich Region

Conjectures that a quark-gluon plasma can be formed in central nuclear collisions at energies $E_{Lab} > 1$ GeV/N rely on the extrapolation from experimental observations at higher energy proton- proton and lower energy nucleus- nucleus collisions. The former data indicate that the mid rapidity region has net baryon numbers close to zero.[24,25] Hence, if nucleons in nuclei behave like free nucleons, nuclei should become transparent at high energies and a clear kinematic separation between the baryon rich fragmentation regions of projectile and target is expected.[26,27] In the few GeV/N bombarding energy range, on the other hand, nuclear stopping has been observed.

Recent calculations based on the inside out cascade yield a strong leakage of baryons into the midrapidity region.[28] Baryon number densities as high as 2/3 of normal nuclear matter density are obtained at mid rapidity; even higher densities are predicted at rapidities closer to the projectile and target.

Hence we may be forced to infer that a zero chemical potential plasma cannot be formed in nuclear collisions at energies as high as E_{lab}=100 GeV/N. Then one would have to deal with a baryon rich plasma at all rapidity values. Unfortunately, theoretical information about the high density (high chemical potential) behaviour of QCD matter is very limited. Lattice QCD calculations of the thermodynamic properties of a plasma containing light quarks are hampered by severe theoretical difficulties: the introduction of fermions on the lattice is at this time only feasible in the quenched approximation.[29] The situation of interest here, a plasma of light quarks and antiquarks plus gluons, can therefore not be studied to date.

The thermodynamic properties of a plasma of light quarks and gluons at finite μ and T may be roughly inferred from perturbative QCD,[30-33] but sizable nonperturbative corrections must be made. In the bag model, the thermodynamical potential of a finite temperature plasma at nonzero chemical potential has been calculated up to third order[32] in α

$$-\Omega = P = \frac{8\pi^2}{45} T^4 + \frac{7\pi^2}{60} n_f T^4 +$$

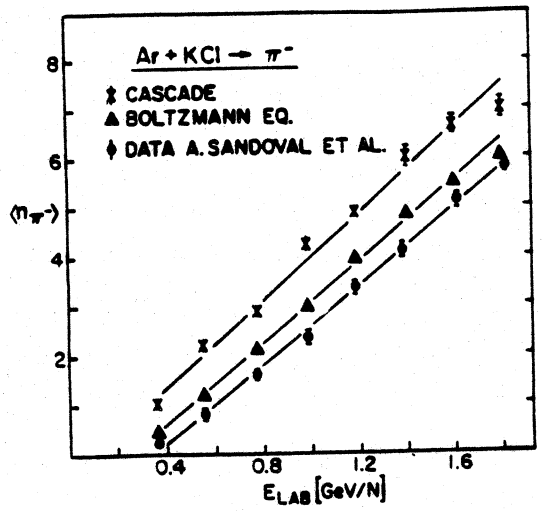

Fig. 9

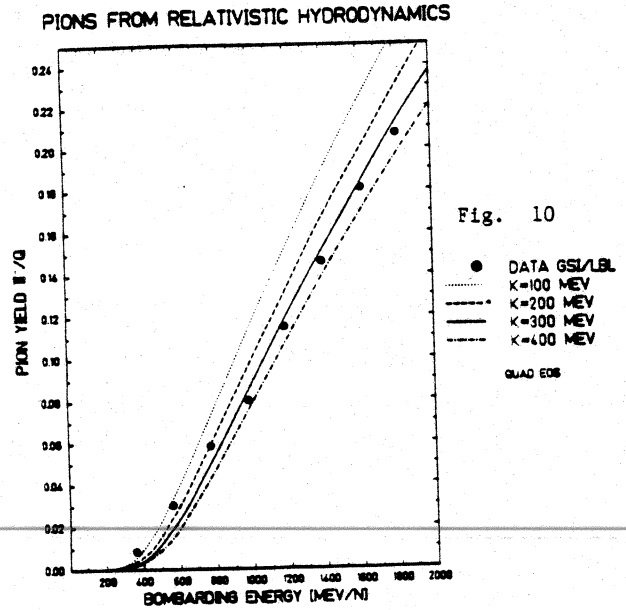

Fig. 10

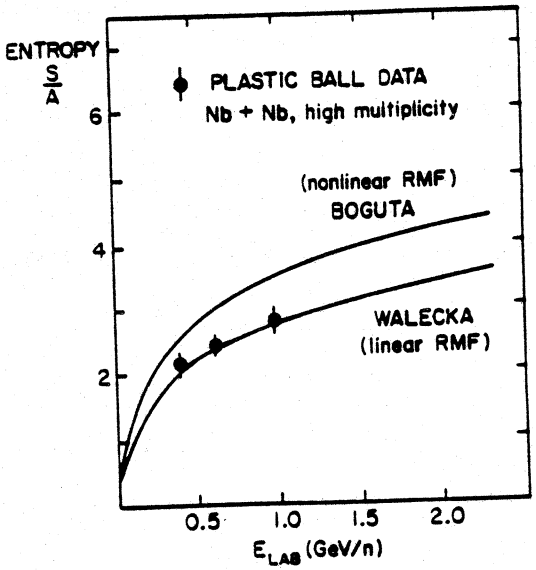

Fig. 11

$$n_f\left(\frac{1}{4\pi^2}\mu^4 + \frac{1}{2}T^2\mu^2\right) - g^2\left(\frac{T^4}{6} + \frac{5n_fT^4}{72} + \frac{1}{8}n_f\left(\frac{\mu^4}{\pi^4} + \frac{2\mu^2T^2}{\pi^2}\right)\right)$$

The g^3 term in this expansion corresponds to the plasmon term in quantum electrodynamics. For small temperatures, this term contributes a finite entropy to the system even at zero temperature thus violating Nernst's theorem. Because of this unphysical behavior we have omitted the plasmon term from further consideration.

Following renormalization group arguments, the running coupling constant α can be written as

$$\alpha = \frac{4\pi}{11 - \frac{2}{3}N_f} \frac{1}{\ell n M^2/\Lambda^2_{MOM}}$$

where N_f is the number of quark flavors involved, M is the effective momentum scale in the matter and Λ_{MOM} is the scale fixing parameter of QCD. The effective momentum scale is estimated to be:

$$M^2 = \frac{4}{3}\sum_i \frac{n_i\langle\vec{p}^2\rangle_i}{\sum_i n_i}$$

where the sum is over all the constituent species present, each with a number density n_i. $\langle\vec{p}^2\rangle_i$ is the thermal average of the three momenta of species i.

For finite μ and T we have evaluated the resulting Bose and Fermion integrals numerically. It is interesting to note that the numerical result can be approximated by

$$M^2 = 4/5\ \mu^2 + 15.622T^2$$

This expression agrees to within a few percent with the correct result. This theory therefore has two free parameters, namely the scale fixing parameter Λ_{MOM} and the energy density of the real vacuum Λ_{VAC}. Λ_{MOM} and Λ_{VAC} can be determined by adjusting the pressure and energy density calculated in this approach at zero chemical potential to SU(N) Yang Mills Monte Carlo data. One obtains[34] Λ_{MOM}=100 MeV and Λ_{VAC}=190

MeV/fm^{-3}. The energy density e, entropy density s, and baryon number ρ of the deconfined quark gluon phase are obtained from the thermodynamical potential via

$$e = -\mu \frac{\partial \Omega}{\partial \mu} - T \frac{\partial \Omega}{\partial T} + \Omega, \quad s = -\frac{\partial \Omega}{\partial T}, \quad \rho = -\frac{1}{3} \frac{\partial \Omega}{\partial \mu}$$

Quark matter is apparently energetically disfavoured compared to ordinary nuclear matter: the minimum energy per baryon of the deconfined phase is about 1.34 GeV, for Λ_{MOM}=100 MeV and Λ_{VAC}=190 MeV/fm^3. Only at densities $\rho > 8\ \rho_0$ would the deconfined state be energetically favorable compared to confined matter at the same density. The energy per particle depends on the choice of Λ_{VAC} and Λ_{MOM}. The energy gap is 0.9 GeV/N when Λ_{VAC} is increased to 450 MeV/fm^3. The energy density at the crossing of the two equations of state is 0.8 - 2.2 GeV/fm^3, hence in the same bulk part as the critical energy density obtained from Monte Carlo data at μ=0.

A first order phase transition can be constructed from the quark- and the hadron phase calculations by equating the pressures of the two phases at the same chemical potential and temperature.[35] The resulting phase coexistence regions are shown in Fig. 12. Observe the rather small gap in the density- temperature plane, in contrast to the wide coexistence regime in the energy density Fig. 14.

To get a rough estimate of the energy density achievable in a nucleus nucleus collision, let us in the following assume[36] that hydrodynamics is valid at higher energies, $E_{lab} > 1$ GeV/N. This extrapolation is questionable at very high energies, $E_{lab} > 20$ GeV/N, because of the longitudinal growth which may lead to the 'transparency'.[24,25,37] In the hydrodynamic calculations, the energy densities attainable depend on the equation of state (EOS) used; see fig. 15. The 'critical' energy densities, e = 1 - 2 GeV/fm^3, may be reached at E_{lab}^{crit} = 4-7 GeV/N, values surprisingly modest compared to the values $E_{lab} > 100$ GeV/N considered to be necessary to form the baryon free plasma.

Graebner et al. have studied the space- time evolution of the zone of highest energy density in the hydrodynamic model;[13] see fig. 16. It is found that with light projectiles high energy densities are

achieved only for times ~ 3 fm/c and only for a rather small number of nucleons (10 - 20) even when heavy target nuclei are used. In particular, the AGS beams (A < 30) may even in the optimistic scenario, assuming complete hydrodynamic stopping, not even result in energy densities of 2 GeV/N, while with a lead beam of only 5 GeV/N, this critical energy density may well be achieved for as many as 200 participating baryons.

The dynamical path of a collision in the ρ-T plane, the phase diagram of hadronic matter, as obtained from a simplified one dimensional treatment of the reaction is depicted in Fig. 13. The initial stage of high compression and excitation is followed quickly by the isentropic expansion of the system. The matter cools only modestly during the dense stage where baryon densities exceed normal nuclear density. At densities below normal density, the system is cooled much more rapidly due to the formation of pions. Also shown in the figure are contours of constant energy densities of 1 and 1.5 GeV/fm^3 of the deconfined phase. Observe that according to the present calculation bombarding energies E_{lab} > 2-4 GeV/N could be sufficient for deconfinement to occur in stopping collisions; see fig. 15. If deconfinement actually would occur at these rather modest energies, the energy gap between confined and deconfined matter would result in temperatures and entropies substantially lower than those calculated under the assumption that deconfinement does not happen. Fig. 17 shows the entropies[38] calculated in the hydrodynamic model assuming that deconfinement i) does and ii) does not occur. The plasma equation of state is used to calculate i) and Walecka's relativistic mean field equation of state is used for ii). The nuclear matter entropy exceeds 4 at E_{lab} > 2 GeV/N. The plasma entropy, on the other hand, is zero at the critical energy necessary to overcome the energy gap, E_{crit} = 2.2 and 4.2 GeV/N for Λ_{VAC}= 190 and 450 MeV/fm^3, respectively. This mechanism of 'cold' plasma production has been discussed previously.[36-39]

It should be noted that none of the discussed possible experimental signatures for the deconfinement transition (dilepton-,[40] photon-,[41] strangeness[42] production) could work in this baryon rich region: these signatures rely on the very high temperatures predicted

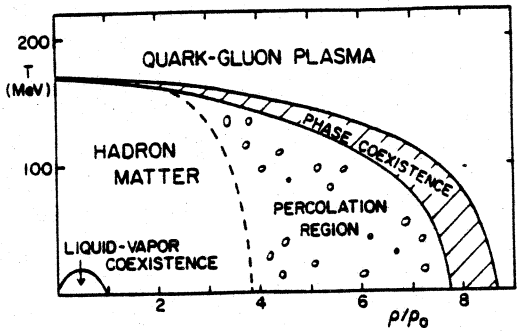

Fig. 12

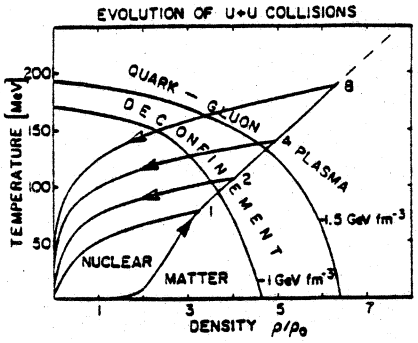

Fig. 13

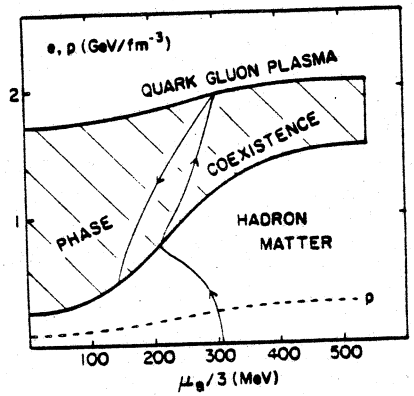

Fig. 14

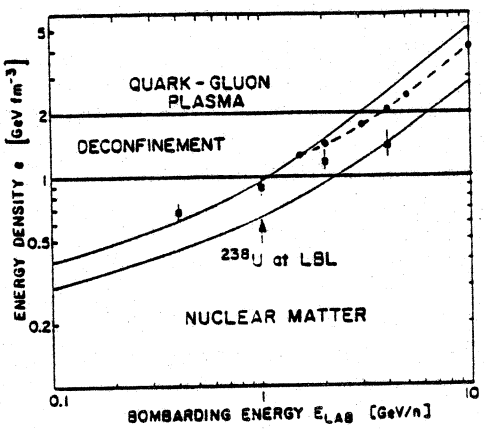

Fig. 15

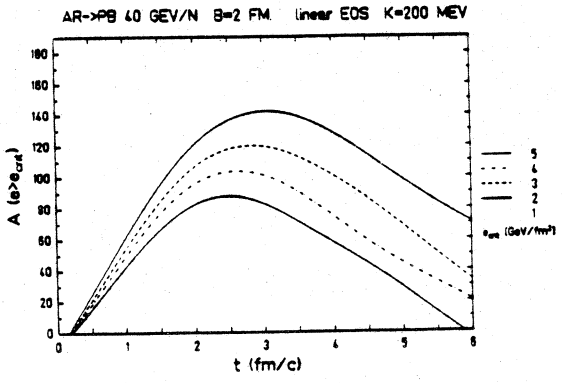

Fig. 16

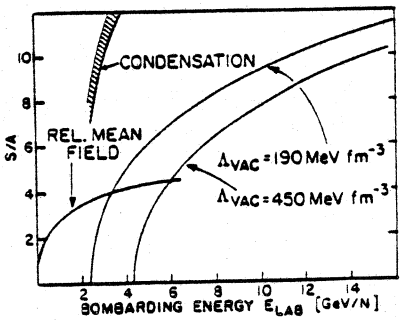

Fig. 17

for the baryon free plasma, while at the same energy density the temperatures in the baryon rich plasma are much lower. Another signature pointed out recently is the production of anti-nuclei.[35]

The plasma entropy increases very fast with the the bombarding energy as compared to the nuclear matter curve. This is due to the repulsive interaction in nuclear matter, in particular in Walecka's model, to be contrasted with the quark-gluon plasma which tends towards asymptotic freedom, i.e. less interactions, with increasing energy density. Hence, the entropy of the plasma phase would exceed the entropy of the confined phase after a transition domain in bombarding energy of about 2 GeV/N. The measurement of the entropy would thus provide an excellent signature for the onset of the deconfinement transition. It could also be very useful for plasma diagnostics because of it's sensitivity to the interactions.

A significant amount of entropy is produced in the condensation discontinuity, which develops at the transition from the quark phase into the hadron phase. It stems from the latent heat (excitation energy) released when the gap energy (0.4 to 0.9 GeV/N) is set free upon recondensation.[38] Some part of the internal energy available is thereby transformed into kinetic energy of the material which is formed behind the condensation discontinuity. The calculated entropy after condensation is depicted in Fig. 17. Observe the large jump from almost zero entropy in the deconfined phase just above the critical bombarding energy to S/A > 7 after recondensation. This increase in fact depends on the vacuum pressure and on the momentum cut off, hence it may be useful for plasma diagnostics. Naturally this threshold increase of S/A would serve as a unique signature for the deconfinement transition. In contrast to the signatures discussed previously, which all rely on the formation of a baryon poor high temperature plasma, this signature does not depend on getting information out of the primordial plasma state before it recondensates but it rather uses the unusual properties of the recondensed matter after the short lived initial state has decayed.

References

1) W. Scheid, H. Müller, W. Greiner, Phys. Rev. Lett. 32, 741 (1974);

J. Hofmann, W. Scheid, W. Greiner, Nuovo Cim. 33A, 343 (1976);

H. Stöcker, J.A. Maruhn, W. Greiner, Z. Physik A290, 297 (1978).

2) H.G. Baumgardt, J.U. Schott, Y. Sakamoto, E. Schopper, H. Stöcker, J. Hofmann, W. Scheid, and W. Greiner, Z. Phys. A273, 359 (1975);

H.G. Baumgardt and E. Schopper, J. Phys. Lett. G5, L231 (1979).

3) R. Stock, H.H. Gutbrod, W.G. Meyer, A.M. Poskanzer, A. Sandoval, J. Gosset, C.H. King, G. King, Ch. Lukner, Nguyen Van Sen, G.D. Westfall, and K.L. Wolf, Phys. Rev. Lett. 44,1243 (1980).

4) H. Stöcker, J.A. Maruhn and W. Greiner, Phys. Rev. Lett. 44, 725 (1980).

5) M. Gyulassy, K.A. Fraenkel, H. Stöcker, Phys. Lett. 110B, 185 (1982).

6) H. Stöcker, G. Buchwald, L.P. Czernai, G. Graebner, J. Theis, J.A. Maruhn, and W. Greiner, Nucl. Phys. A387, 205 (1982), and Nucl. Phys. A400, 63 (1983);

G. Buchwald et al., Phys. Rev. C28, 2349(1983).

7) J. I. Kapusta and D. Strottman, Phys. Lett. 103B, 269 (1981);

J. Cugnon, J. Knoll, C. Riedel, and Y. Yariv, Phys. Lett. 109B, 167 (1982).

8) H.G. Ritter, H.A. Gustafsson, H.H. Gutbrod, B. Kolb, H. Löhner, B. Ludewigt, A.M. Poskanzer, T. Renner, H. Riedesel, A. Warwick, F. Weik, H. Weiman, Lawrence Berkeley Laboratory preprint 16110 (1983) and Proceedings of the International Conference on High Energy Nuclear Physics, p. 275, J. Erö (ed.), Balatonfüred, Hungary, June 1983.

H.A. Gustafsson, et al., Phys. Rev. Lett. 52, 1590 (1984);

P. Danielewicz, et al., LBL-preprint (1984) unpublished;

D. Beavis et al., UC Riverside preprint (1984) unpublished.

9) Y. Yariv and Z. Fraenkel, Phys. Rev. C20, 2227 (1979); C24, 488 (1981);

V.D. Toneev, K.K. Gudima, Nucl. Phys. A400, 173 (1983).

J. Cugnon, D. Kinet, J. Vandermeulen, Nucl. Phys. A379, 553 (1982);

J. Cugnon, T. Mituzani, J. Vandermeulen, Nucl. Phys. A352, 505 (1981).

10) J.J. Molitoris, J.B. Hoffer, H. Kruse, H. Stöcker, Phys. Rev. Lett. 53, 899 (1984)

J.J. Molitoris, H. Stöcker, to be submitted to Phys. Rev. C.

11) A.R. Bodmer, C.N. Panos, Phys. Rev. C15 (1977) 1342;

A.R. Bodmer, C.N. Panos, A.D. MacKellar, Phys. Rev. C22, 1025 (1980);

A.R. Bodmer, C.N. Panos, Nucl. Phys. A356, 517 (1981).

A.R. Bodmer, Proc. 5th High Energy Heavy Ion Study, May 1981, p. 648, LBL-12652, Berkeley, California.

12) L. Wilets, E.M. Henley, M. Kraft, A.D. MacKellar, Nucl. Phys. A282 (1977) 341; L. Wilets, Y. Yariv, R. Chestnut, ibid. A301, 359 (1978);

D.J.E. Callaway, L. Wilets, Y. Yariv, ibid. A327, 250 (1979).

13) G. Buchwald, G. Graebner, J. Theis, J. Maruhn, W. Greiner, and H. Stöcker, Phys. Rev. Lett., 52, 18 (1984).

G. Graebner, et al., to be published.

14) H. Kruse, B. Jacak, H. Stöcker Phys. Rev. Lett. in press.

15) P. Danielewicz and M. Gyulassy, Phys. Lett. 129B, 283 (1983).

16) G. Bertsch, H. Kruse, and S. Das Gupta, Phys. Rev. C29, 673 (1984).

17) H. Kruse, B. Jacak, J.J. Molitoris, G.D. Westfall, H. Stöcker, submitted to Physics Letters.

18) S. Nagamiya, M.C. Lemaire, E. Moeller, S. Schnetzer, G. Shapiro, H. Steiner, I. Tanihata, Phys. Rev. C24 (1981) 971;

B. Jacak, G.D. Westfall, C.K. Gelbke, L.H. Harwood, W.G. Lynch, D.K. Scott, H. Stöcker, M.B. Tsang, T.J.M. Symons, Phys. Rev. Lett. 51, 1846 (1984).

19) R. Stock, R. Bock, R. Brockmann, J.W. Harris, A. Sandoval, H. Stroebele, K.L. Wolf, H.G. Pugh, L.S. Schroeder, M. Maier, R.E. Renfordt, A. Dacal, M.E. Ortiz, Phys. Rev. Lett. 49, 1236 (1982);

A. Sandoval et al., ibido, 45, 874 (1980);

J.W. Harris et al., GSI-preprint (1984).

20) R.E. Renfordt, D. Schall, R. Bock, R. Brockmann, J.W. Harris, A. Sandoval, R. Stock, H. Stroebele, D. Bangert, W. Rauch, G. Odyniec, H.G. Pugh, L.S. Schroeder, Phys. Rev. Lett. 53,8(1984)763.

21) J.J. Molitoris, H. Stöcker, to be published.

22) J.D. Walecka, Ann. Phys. (N.Y.) 83, 491 (1974).

23) R. Y. Cusson, P.G. Reinhard, H. Stocker, M.R. Strayer, W. Greiner, to be published.

24) N.N. Nikolaev, Sov. J. Part. Nucl. 12,63 (1981)

25) S. Pokorski and L. Van Hove, Nucl. Phys. B86 (1975) 243.

26) J.D. Bjorken, Phys. Rev. D27 (1983) 140.

27) R. Anishetty, P. Koehler, L. McLerran, Phys. Rev. D22 (1980) 2293.

28) K. Kajantie, P. Raitio, P.V. Ruuskanen, Nucl. Phys. B222 (1983) 152.

29) J. Kogut et al., Urbana Preprint (1983);
J. Engels, F. Karsch, CERN preprint (1983);
T. Celik, J. Engels, H. Satz, Bielefeld preprint (1983).

30) B.A. Freedman, L.D. McLerran, Phys. Rev. D16 (1977) 1169.

31) S.A. Chiñ, Phys. Lett. 78B (1978) 552.

32) J.I. Kapusta, Nucl. Phys. B148 (1979) 461.

33) E.V. Shuryak, Phys. Rep. 61 (1980) 71.

34) H. Satz, Bielefeld preprint (1982).

35) P.R. Subramanian, W. Greiner, D. Hahn, H. Stocker, U.Heinz, to be published;
U. Heinz, P.R. Subramanian, W. Greiner, Z. Physik, in print.

36) H. Stöcker, G.F. Graebner, J.A. Maruhn, W. Greiner, Phys. Lett. 95B (1980)192.

37) M. Gyulassy, LBL preprint 16292 (1983).

38) H. Stocker, Nucl. Phys. A 418 587 (1984).

39) T.S. Biro, J. Zimanyi, Nucl. Phys. A395 (1983) 25.

40) G. Domokos, J. Goldman, Phys. Rev. D23 (1981) 203.

41) K. Kajantie, H.I. Mietinnen, Z. Physik C9 (1981) 341, and C14 (1982) 357.

42) P.Koch, J. Rafelski, W. Greiner, Phys. Lett. 123B (1983) 151;
T.S. Biro, J. Zimanyi, Phys. Lett. 113B (1982) 6;
J. Rafelski, B. Muller, Phys. Rev. Lett. 48 (1982) 1066.